2011 IEEE International Conference on Robotics and Automation
Shanghai International Conference Center
May 9-13, 2011, Shanghai, China

Grasping From the Air: Hovering Capture and Load Stability

Paul E. I. Pounds, *Member, IEEE*, Daniel R. Bersak, and Aaron M. Dollar, *Member, IEEE*

***Abstract*— This paper reports recent research efforts to advance the functionality of Unmanned Aerial Vehicles (UAVs) beyond passive observation to active interaction with and manipulation of objects. The archetypical aerial manipulation task — grasping objects during flight — is difficult due to the unstable dynamics of rotorcraft and coupled object-aircraft motion. In this paper, we analyze key challenges encountered when lifting a grasped object and transitioning into laden free-flight. We demonstrate that dynamic load disturbances introduced by the load mass will be rejected by a helicopter with PID flight control. We determine stability bounds in which the changing mass-inertia parameters of the system due to the grasped object will not destabilize this flight controller. The conditions under which transient partial contact mechanics of objects resting on a surface will not induce instability are identified. We demonstrate grasping and retrieval of a variety of objects while hovering, without touching the ground, using the Yale Aerial Manipulator testbed.**

I. Introduction

Unmanned Aerial Vehicles (UAVs) have rapidly evolved into capable mobility platforms able to maneuver, navigate and survey proficiently. A natural progression is to advance beyond simple motion and observation to interaction with objects and the fixed environment. Of specific interest is grasping and retrieving objects while hovering, combining terrestrial robot manipulation capabilities with the range, speed and vertical workspace of flying vehicles. This could make possible novel applications for UAVs, such as search and retrieval in rough or inaccessible terrain or networked aerial logistical supply chains over large areas.

Several limited examples of flying vehicles physically interacting with objects have been demonstrated, such as in-flight refueling [1], [2] and the transport of slung loads, both individually and cooperatively [3], [4], [5], [6]. In these examples the interacting object is either not acquired automatically (such as a load attached by a human operator on the ground) or highly structured (e.g. refueling booms with optical markers). Efforts to develop autonomous helicopter UAV payload acquisition have relied on structuring of the target object to simplify the task, such as a hanging magnet at the end of a probe to collect ferrous objects [7], [8], or a hook at the end of a probe to snag a hoop on an object [9].

In contrast to more constrained approaches, our aim is to demonstrate generalized object retrieval and transport of unstructured objects from aerial platforms. The most substantial aspects of this problem can be classified into approach and alignment, grasp performance, aircraft stability during object contact, and laden flight stability.

Fig. 1. Yale Aerial Manipulator capturing a block in hover.

We address the first two issues by incorporating a highly adaptive compliant grasper mounted ventrally on a helicopter airframe. This enables the aircraft to acquire a variety of target objects even in the presence of large positioning errors due to aerodynamic disturbances [10], and remain stable when coupled to the payload on the ground [11]. Laden aircraft stability, object contact and transition to free flight are the primary focus of this paper.

Instability and fragility of hovering vehicles encourage an "avoid at all costs" approach to contact with surroundings. Landing and take-off generally involve rapidly transitioning through partial contact conditions, with minimal time in intermediate states between static and dynamic stability, where the danger of ground collision is high. For grasping and manipulating external objects, operation in these regimes is required — both when grasping objects and in the process of lifting a target clear of the ground. The stability of the aircraft in coupled and partial contact with ground, and once airborne with payload, must be analyzed and assured.

In this paper, we discuss key challenges of grasping from a hovering vehicle and present our experimental platform, the Yale Aerial Manipulator (Fig. 1). A dynamic model of the longitudinal and pitch dynamics of a helicopter with a PID attitude controller is used to determine object mass and placement limits for closed-loop stability and cyclic control saturation bounds. We show both analytically and experimentally (using a PID-stabilized helicopter) that the system is robust to load step disturbances similar to those applied by a captured object. We experimentally show stable hover of a helicopter coupled to an object fixed to ground, analysis of which was presented in [11]. Finally, we discuss transition to free flight and demonstrate retrieval of a number of unstructured objects by the helicopter in stable hover.

Manuscript received 15 Sept 2010. This work was supported in part by the Office of Naval Research grant N000141010737.

P. E. I. Pounds, D. R. Bersak, and A. M. Dollar are with the Department of Mechanical Engineering and Materials Science, School of Engineering and Applied Science, Yale University, New Haven, CT USA.
(e-mail: {firstname.lastname}@yale.edu).

Fig. 2. Yale Aerial Manipulator with gripper and fixed gear.

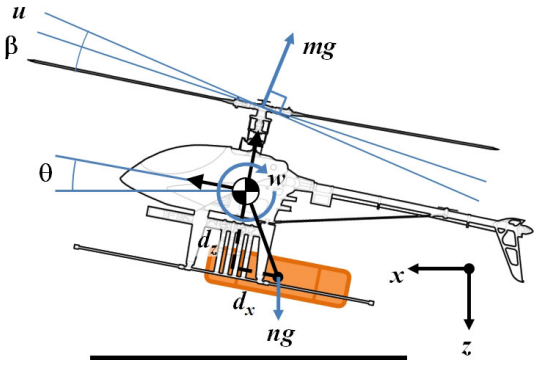

Fig. 3. Planar aircraft dynamics free body diagram.

II. Grasping From a Hovering Vehicle

The grasping task can be divided into phases: approach and alignment to the target, grasping hover while coupled to an object resting on the ground, partial coupling during liftoff, and departure. Each phase poses specific challenges.

Disruptive aerodynamic surface effects make near-ground position-keeping outdoors more difficult than hover in free air [10]. The wake of the rotor is contained by the surface underneath it, creating a repelling cushion of air referred to as 'ground effect'. As a rotorcraft moves laterally through ground effect, the deflected wake is pushed ahead of the aircraft and can be entrained and recirculated by the rotor, causing a ground vortex. When the vortex enters the rotor, the thrust decreases rapidly; together these create an instability that causes the aircraft to bounce on descent and then drift and plunge from wake interactions. Typical UAV helicopter free-air station-keeping accuracy is on the order of tens of centimeters; the Rotomotion SR-100 UAV (7 kg, 2 m rotor) has a reported 20 cm position-keeping accuracy [9]. In practice, UAV hovering is not yet sufficiently precise to enable grasping with a rigid manipulator.

When the vehicle is in position and has a secure grasp on the target, its flight dynamics become coupled to the ground through forces transmitted by the gripper. Certain ratios of lateral and angular coupling stiffness can destabilize the aircraft [11]. As thrust increases and the surface normal force decreases, this coupling must remain well-conditioned.

Once the object is lofted clear of the ground, the added load must not destabilize the helicopter. The added mass changes physical parameters of the system — the net mass, moment of inertia, and location of the Center of Gravity (CoG) of the vehicle are all altered. Flight controllers tuned for specific aircraft parameters may not accommodate changing plant mid-flight — interaction between the controller and changing system parameters must not lead to instability. Aircraft mass change mid-flight is usually negative, as fuel is consumed or payload is deployed; the effects of directly attaching payload to a helicopter mid-flight are unexplored.

A. Yale Aerial Manipulator

Our experimental platform, the Yale Aerial Manipulator, consists of a compliant underactuated manipulator, based on the SDM Hand [14], mounted ventrally between the skids of a 4 kg, 1.5 m rotor, T-Rex 600 ESP radio control helicopter (Align, Taiwan) (Fig. 3). The gripper consists of four fingers with two elastic joints each, actuated by a parallel tendon mechanism that balances loads across each digit; it has a grasp span of 115 mm. The special characteristics of the hand design — open-loop adaptive grasping, wide finger span, insensitivity to positional error – closely match the challenges associated with the UAV manipulation task, allowing for a very simple, light-weight mechanism, without the need for imposed structural constraints on the load. The gripper unit and landing gear are modular, allowing for alternative payloads, retractable skids and other fittings to be attached.

III. Flight Stability With Payload

Much work has been done to control autonomous rotorcraft flight attitude, and the dynamics of helicopters in hover are well understood [7], [12], [15]. Due to the largely decoupled lateral and longitudinal dynamics of helicopters around hover, a planar linear model is useful for analyzing the stability of both the free-air and ground-coupled systems. In this paper, longitudinal dynamics are considered, but the analysis is equally applicable to lateral flight near hover.

A. Helicopter Dynamic Model

The rigid-body dynamics of the linearized planar helicopter in hover are[1] (Fig. 3):

$$m\ddot{x} = -mg\beta - mg\theta - mgu \quad (1)$$

$$\mathrm{I}\ddot{\theta} = mgh\beta + mghu + w \quad (2)$$

where m is the mass of the helicopter, I is the rotational inertia in pitch, g is acceleration due to gravity, x, z and θ are the longitudinal, vertical and angular position of the CoG with respect to the inertial frame, h is the rotor height above the CoG, β is the first harmonic longitudinal rotor flapping angle, u is the cyclic pitch control input, and w is the pitch moment applied by the payload.

All helicopters exhibit rotor flapping [16]; we consider a teetering rotor free to pivot at the center like a see-saw . In horizontal motion, the on-coming wind causes an imbalance in lift between the blades on either side of the rotor disc. This causes the rotor plane to pitch upward, changing the angle of attack of each blade until a new equilibrium is reached.

[1]Rotor thrust is taken as constant, exactly canceling helicopter weight.

The angled rotor directs some of its thrust aft, slowing the helicopter and producing a pitching moment. Flapping dynamics are a crucial part of helicopter stability analysis, even at low speeds [12]. The rotor pitch response time is extremely fast, and so it can be represented analytically, without need for additional states.

At low speeds, the flapping angle produced by a 'see-saw' teetering rotor head is an approximately linear combination of the longitudinal translation and pitch velocities:

$$\beta = q_1 \dot{x} - q_2 \dot{\theta} \tag{3}$$

where q_1 and q_2 are constant parameters of the rotor [12].

In the case of rotor heads with Bell-Hiller stabilizer bars, the flapping angle is augmented by that of the sub-rotor, multiplied by the mechanical advantage of the stabilizer linkage transmission K [15]:

$$\beta' \quad = \quad \beta + K(q_{1s}\dot{x} - q_{2s}\dot{\theta}) \tag{4}$$

where q_{1s} and q_{2s} are the stabilizer flapping parameters. Together, the stabilized rotor dynamics are homologous to that of a conventional rotor with slower time constants:

$$\beta' = (q_1 + Kq_{1s})\dot{x} - (q_2 + Kq_{2s})\dot{\theta} \tag{5}$$

Thus, we need not distinguish between the two in this analysis.

Helicopter pitch and longitudinal motion are strongly interdependent, but vertical motion is effectively decoupled from these around hover. Solving the longitudinal translation-pitch equations together produces a single-input-single-output transfer function between the cyclic control input and the pitch angle in free flight:

$$H = \frac{m^2 ghs}{\mathrm{I}Gs^2 + mghq_2Gs - m^2g^2hq_1(q_2 s - 1)} \tag{6}$$

where $G = (ms + q_1 mg)$, the dynamics associated with translation due to pitch.

B. Flight Stability With Payload Mass

While several autonomous helicopters have flown with tethered loads [3], [5], [6], the slung configuration is specifically designed to decouple the motion of the load from the helicopter, and separate the timescales of the attitude and tether-pendulum dynamics [4]. In the case of grasped loads, the payload is directly coupled to vehicle pitch and lateral motions – the closed-loop system must be shown to remain stable in the expected range of system mass and inertia.

Level flight of helicopters is regulated by an onboard flight controller, maintaining $\theta = 0$. A common architecture used in UAV rotorcraft is Proportional-Integral-Derivative control. The transfer function for a PID controller has the form:

$$C = k\left(1 + k_i \frac{1}{s} + k_d s\right) \tag{7}$$

where k is the control gain, and k_i and k_d are the integral and differential control parameters.

The stability of the closed-loop system can be assessed by examining the transfer function characteristic polynomial. The polynomial is the sum of the products of the numerators (subscript n) and denominators (subscript d) of C and H:

$$C_n H_n + C_d H_d \tag{8}$$

Substituting (6) and (7), this becomes:

$$s^3 + \left(\frac{mgh}{\mathrm{I}}(q_2 + kk_d) + q_1 g\right) s^2 + k\frac{mgh}{\mathrm{I}} s + \frac{mgh}{\mathrm{I}}(kk_i + q_1) \tag{9}$$

As the unladen helicopter is stable in free air, this polynomial is known to be stable.

Adding payload to the aircraft changes three key parameters: m, the mass of the helicopter, I, the rotational inertia of the helicopter, and h, the height of the rotor plane above the CoG. Changes to these values depend on three attributes of the acquired load: n, the mass of the payload, and d_x and d_z, the longitudinal and vertical offsets of the payload mass from the vehicle CoG. The adjusted parameters are calculated by:

$$m' \quad = \quad m + n \tag{10}$$

$$\mathrm{I}' \quad = \quad \mathrm{I} + \mathrm{I}_n + n(d_x^2 + d_z^2) \tag{11}$$

$$h' \quad = \quad h + \frac{n}{n+m} d_z \tag{12}$$

where I_n is the rotational inertia of the added payload[2].

The continued stability of the characteristic polynomial can be assessed using the Routh-Hurwitz criterion [11]. The criterion states that for a dynamical system to be stable, its characteristic polynomial must have all positive coefficients, and that leading entries in the Routh-Hurwitz array derived from those coefficients must be positive. In the case of a third order polynomial:

$$s^3 + a_1 s^2 + a_2 s + a_3 \tag{13}$$

The lead elements of the array are given by:

$$b_1 \quad = \quad (a_1 a_2 - a_3)/a_1 \tag{14}$$

$$c_1 \quad = \quad a_3 \tag{15}$$

Mass added to the helicopter is always positive. While in principle d_z may be arbitrarily positive or negative, the structure of most helicopters precludes adding mass sufficiently far above their centers of gravity such that $h' < 0$. Thus, the characteristic polynomial coefficients are always positive.

Therefore, as $c_1 = a_3$, only array element b_1 can change signs. From (14) the stability condition becomes:

$$a_1 a_2 - a_3 > 0 \tag{16}$$

Substituting the characteristic polynomial coefficients and (10)–(12) and rearranging, this can be expressed as:

$$\frac{m'gh'}{\mathrm{I}'} > \frac{q_1 g - q_1 gk + kk_i}{(q_2 + kk_d)k} \tag{17}$$

Note that the right-hand side of the inequality consists only of constant terms of the aerodynamics and controller; we denote this constant P. All mass and inertial parameters

[2]Note that all rotations are considered to occur around the unloaded CoG of the helicopter; offset mass effects are accounted for in the load bias torque.

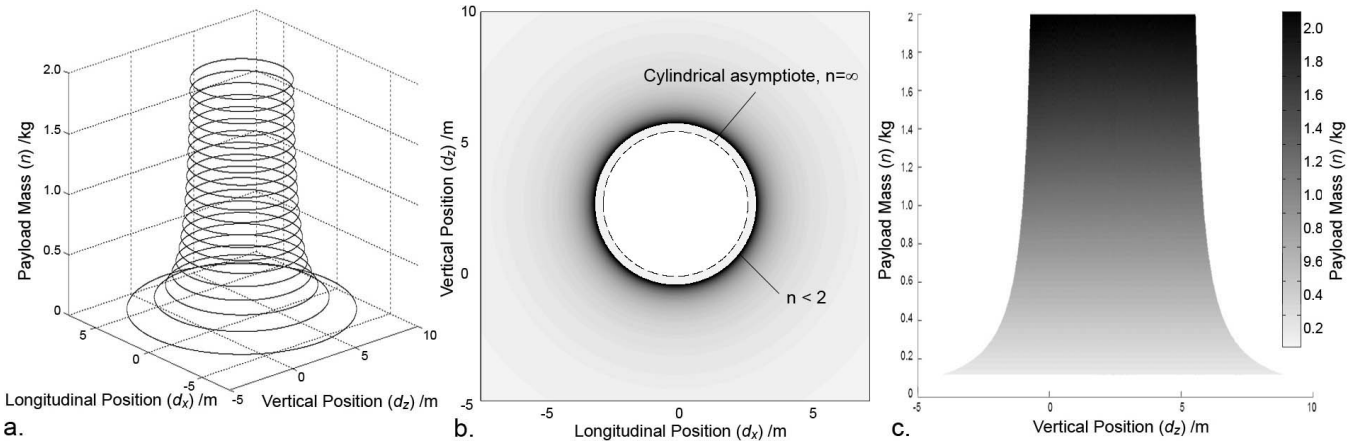

Fig. 4. Stability region for offset loads: a. Position-mass height map, b. Vertical position-mass elevation, c. Isometric with mass isoclines.

modified by changing payload appear on the left-hand side of the inequality; we denote this variable Q. Thus, any loading configuration will be stable provided that $Q > P$. This stability criterion Q is a physical characteristic of the vehicle relating rotor cyclic torque to rotational acceleration, and has units of s^{-2}. It appears in (2) as the open-loop pitch transfer function gain:

$$\frac{\theta(s)}{\beta(s)} = Q\frac{1}{s^2} \tag{18}$$

Stability criterion (17) can be directly transformed into a relation between the three load attributes:

$$\frac{(m+n)g(h+\frac{n}{m+n}d_z)}{\mathrm{I}+n(d_x^2+d_z^2)} > P \tag{19}$$

The rotational inertia of the load, I_n, is considered to be very small and is treated as zero. This relation can be solved to compute the range of permissible offsets, given a known payload mass, or conversely for maximum load given a payload position envelope.

The surface of the stability bound $Q = P$ is a hyperbolic cylindrical funnel (Fig. 4a and 4b); loading configurations under this surface are stable. The funnel is centered around $d_z = g/2p$ with a circular asymptote (Fig. 4b) of radius:

$$\sqrt{\frac{4ph+g^2}{4p^2}} \tag{20}$$

Within this circle, no amount of added mass will destabilize the vehicle.

In practice, the distribution of payload on a helicopter with a ventral gripper has much less variation in d_z than d_x due to the fixed height of the gripper below the helicopter. The boundary of the cross-section through the stable configuration region can be determined by holding d_z fixed:

$$d_x^2 < \left(\frac{mgh-p\mathrm{I}}{p}\right)\frac{1}{n}+\frac{gh+gd_z-pd_z^2}{p} \tag{21}$$

Correspondingly, the hyperbolic asymptote (Fig. 5) is given by:

$$d_x = \sqrt{\frac{h+d_z-pd_z^2}{p}} \tag{22}$$

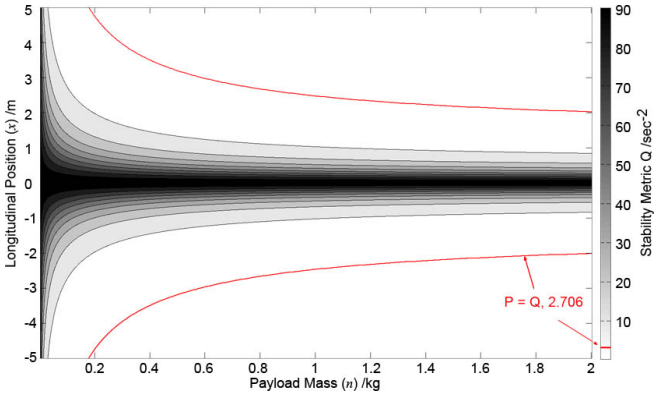

Fig. 5. Stability metric position-mass isoclines, $d_z = 0.2$ m.

Similarly to (20), any mass (up to the capacity of the vehicle) may be added without destabilizing the aircraft.

Beyond predicting stability, the Q metric provides an indication of the robustness of the system. The value of Q decreases monotonically as d_x and n approach the stability bound at $Q = P$ (Fig. 5).

C. Load Offset Rejection

Given loading conditions known not to destabilize the vehicle in flight, it can be shown that bias torque loads accompanying payloads offset from the CoG will be rejected by the controller. Solving the linearized equations in the s-domain, the aircraft pitch angle can be written as a sum of the open loop system transfer function and a filtered load disturbance (Fig. 6):

$$\theta(s) = \frac{m^2ghsu(s)+Gw(s)}{\mathrm{I}Gs^2+mghq_2Gs-m^2g^2hq_1(q_2s-1)} \tag{23}$$

where $G = (ms+q_1mg)$. This can be rewritten as:

$$\theta(s) = \frac{H_n}{H_d}u(s)+\frac{G}{H_d}w(s) \tag{24}$$

As the system is linear, the two transfer functions can be considered separately. In closed-loop control with linear compensator C, the transfer function between the disturbance

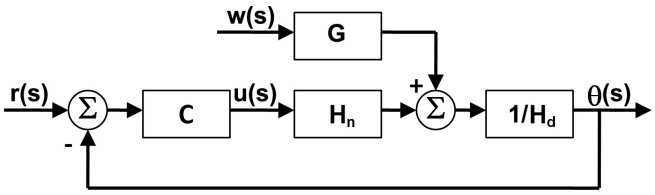

Fig. 6. System disturbance block diagram.

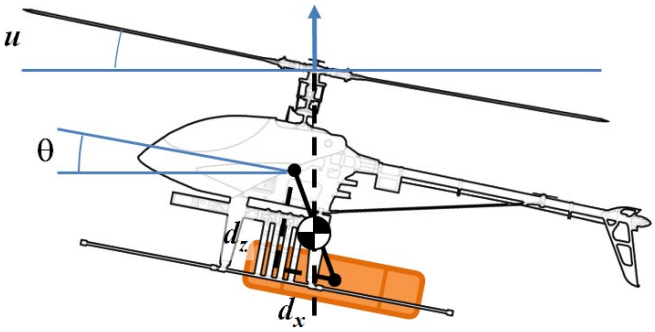

Fig. 7. Cyclic trim balance angle.

and the output is:

$$\frac{\theta(s)}{w(s)} = \frac{G}{H_d + CH_n} \tag{25}$$

The denominator is identical to that of the stabilized closed loop transfer function between reference, r, and the output:

$$\frac{\theta(s)}{r(s)} = \frac{CH_n}{H_d + CH_n} \tag{26}$$

Thus, the stability of the disturbance response is not dependent upon G. Given a compensator that successfully regulates the attitude dynamics around hover, small torque bias disturbances that do not take the system into the nonlinear regime or saturate the cyclic control margin will be rejected. However, the finite response time of the compensator can still result in large transient responses, such as when an object is dropped mid-flight, potentially leading to sufficiently large excursions to result in a crash [3].

D. Flight Trim Under Load

When an unbalanced load is added to the helicopter, the trim position during hover is affected. From (2), by inspection the equilibrium condition occurs when:

$$m'g\beta + m'gu = \frac{w}{h'} \tag{27}$$

Substituting into (1), the lateral acceleration becomes:

$$m'\ddot{x} = -\frac{w}{h'} - m'g\theta \tag{28}$$

As the onboard controller seeks to return θ to zero in equilibrium, this will result in constant longitudinal acceleration. Human pilots trim for this imbalance by allowing non-zero values of θ in hover.

For simple weight load torque $w = ngd_x$, this gives the trim condition:

$$mg\theta = ng\frac{d_x}{h'} \tag{29}$$

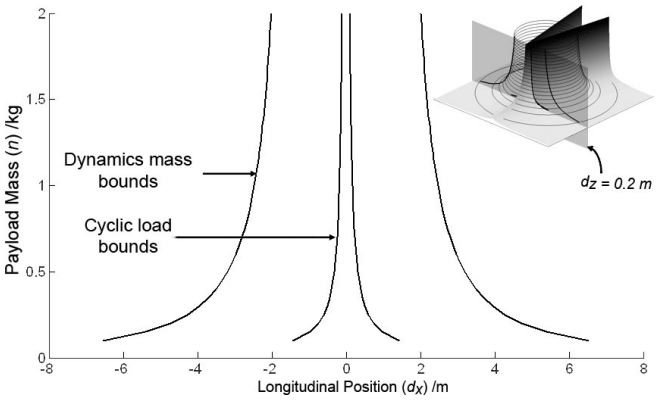

Fig. 8. Longitudinal position-mass stability bounds for $d_z = 0.2$ m.

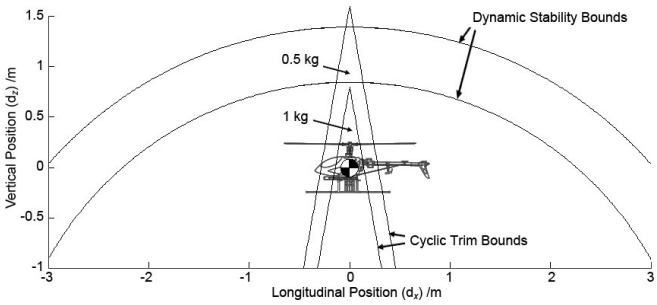

Fig. 9. Position stability bound isoclines for 0.5 and 1 kg loads.

which yields:

$$\theta = \frac{d_x}{h\frac{m}{n} + h + d_z} \tag{30}$$

This is the angle subtended by the rotor axis and the combined CoG – the trim condition where the net mass is suspended directly below the rotor hub in hover (Fig. 7).

If the mass and attachment position of the payload is known, the flight controller can be instructed to maintain this pitch angle and so avoid unbounded position drift.

For level hover, $u = -\theta$, and this angle must always be within the helicopters cyclic control range. If the cyclic control saturates, the helicopter will be uncontrollable. Typical cyclic range for a small scale helicopter is $\pm 10°$ [16]. The cyclic range places a static load bound on the allowable mass distribution, with an asymptote at:

$$d_x = \theta(h + d_z) \tag{31}$$

where $d_z < h$.

Combined with (22), the cyclic trim bound of (30) describes the range of allowable payload mass and position parameters (Fig. 8). Of the two, the cyclic trim applies a much stricter limit on payload position (Fig. 9). The limited cyclic control range ensures that statically stable payload will not adversely effect dynamic stability of the aircraft.

IV. Payload Stability Experiments

To demonstrate aircraft stability under PID control after payload capture, two experiments were performed: the first to demonstrate robustness of the flight controller to step

Fig. 10. Yale Aerial Manipulator with payload rail and fixed gear.

TABLE I
AIRCRAFT PARAMETERS

Aerodynamics and Mass Parameters					
g	9.81	ms^{-s}	m	4	kg
h	0.2	m	I	0.1909	kgm
q_1	0.0039		d_z	0.275	m
q_2	0.0266				
PID Control Parameters					
k	0.24		k_d	1.7	
k_i	0.7				

loads and the second to assess stability of the controller with changing payload positions.

The helicopter is fitted with a Helicommand Profi flight stability system that employs a PID attitude controller, with known parameters. It also controls height above ground and position drift using optical feedback, but this function is turned off during experiments to avoid interference with dynamic response measurements. Flight attitude is measured by a 3DM-GX3-25 inertial measurement unit (Microstrain, Vermont USA) and transmitted via bluetooth to an off-board laptop. Aircraft and control parameters are given in Table I.

A 0.48 m long aluminum rail is mounted ventrally between the helicopters skids, 0.2 m below the unladen aircraft CoG, aligned with the aircraft x axis (Fig. 10). The rail has mounting holes every 25.4 mm to which a fixed mass or remote-triggered electromagnet may be secured, allowing loads to be shifted between tests, or dropped mid-test.

A. Dynamic Load Bias Test

In the first experiment, a 0.125 kg test mass is dropped from a range of mounting positions under the helicopter to produce step load disturbances. From (27), rotor cyclic control is analogous to applied torque. By trimming the aircraft in flight with the test mass in place and then releasing it, the pitch dynamics will emulate the effect of instantaneously applying an unbalanced payload, which is difficult to achieve in practice.

Prior to the drop, the helicopter is autonomously held stationary out of ground effect, at a pitch angle that cancels the moment of the test mass. As the drop is triggered, the horizontal position control of the flight stabilizer is simultaneously disabled. Five trials were performed, with the test mass starting 50.8 mm forward of rotor axis and moved 50.8 mm further away each time. The resulting pitch motion of the aircraft shows that the system successfully rejects step

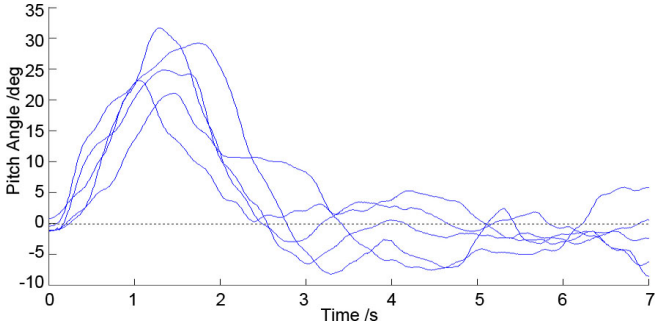

Fig. 11. Normalized unit load bias step responses.

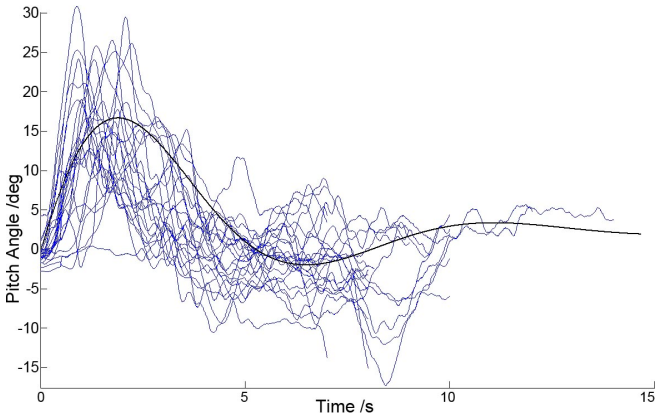

Fig. 12. Normalized shifted mass drop step responses.

biases (Fig. 11). As expected from (28), however, the lateral motion of the aircraft was unbounded and experiment settling time was limited by available flight space.

B. Added Mass Flight Stability Test

In the second experiment, the stability of the system with different fixed mass configurations is tested. A weight is attached at a range of locations on the mounting rail, and the helicopter is trimmed for the added mass, along with a small test mass at a set location. Experiment setup is as previously: the craft is kept stationary under autonomous control until the test mass is released to induce a step response. In total, 24 trials were performed, with the fixed mass moved 25.4 mm further from the rotor axis every third trial.

From (25), the expected disturbance step response is a one zero, three pole system with a decaying oscillation period of 7.6 s. Due to limited airspace for testing, not all tests could be allowed to continue to complete settling, as the aircraft translated at a high rate from unbalanced trim after the drop.

In outdoor flight, the pitch motion of the aircraft is noisy, making estimation of the system poles difficult. Some cross-coupling between pitch and roll was observed; a least-squared regression on roll measurements identified a linear coupling factor and phase lag that was used to remove its influence in the pitch measurement.

The aggregate dynamics tracked the predicted step response of the system (Fig. 12), with a slightly shorter oscillation period than predicted ($\sim$5 s). Given the noise in the measurements, the oscillatory poles identified from the step responses were widely spaced; these identified poles

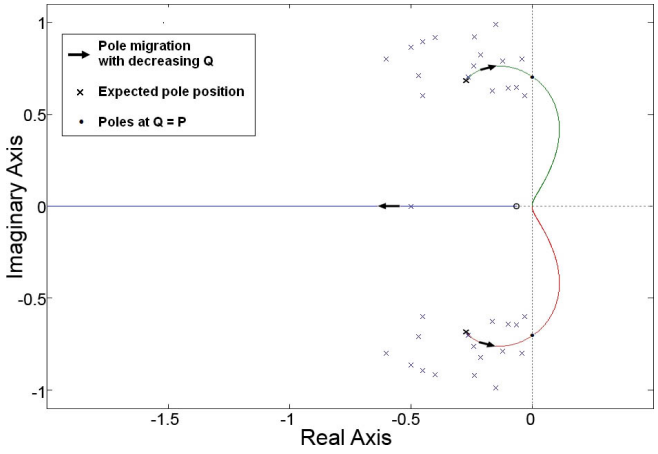

Fig. 13. Shifted mass step response pole positions.

and zeros are shown in superimposed on the root locus with respect to changing Q in figure 13. As Q decreases, the system is expected to become more oscillatory, crossing the axis when $Q = P$. However, the limitation imposed by (30) prevented the mass from being displaced far enough to discern any trend towards incipient instability.

V. Grasping While Hovering

A. Hovering Coupled to a Fixed Object

It was shown in an earlier analysis that a hovering helicopter grasping an object fixed to the ground with a compliant gripper should be stable for certain ratios of lateral and angular gripper stiffness, k'_x and k'_θ [11]. For a generalized stiffness model of the gripper forces and torques applied to the airframe, $F_x = k'_x x$ and $\tau = k'_\theta \theta$, the stability bound was:

$$k'_x < \frac{mh}{\mathrm{I}(h + q_1 d_z)} k'_\theta + g \left(\frac{mh}{\mathrm{I}(h + q_1 d_z)} \right)^2 \qquad (32)$$

The Aerial Manipulator gripper system stiffnesses are small, and therefore the final term of (32) dominates ensuring the inequality is satisfied, and the system remains stable.

To validate the stability of the aircraft in coupled hovering under PID control, we used the aerial manipulator platform to grasp a wood block attached to the ground (Fig. 14). The aircraft was flown into position under control of a human safety pilot with landing gear retracted and then switched to autonomous PID hover as the gripper was closed. For the duration of the experiment, the hover thrust was maintained and the pilot did not issue commands to the vehicle.

After achieving a grasp the vehicle remained stable; the aircraft gripper was released after 32 seconds (Fig. 15 and Fig. 14d). The slow oscillation of the aircraft during contact hover is thought to be due to wind eddy currents in the outdoor test facility. The experiment was repeated, with the aircraft hovering in contact for 26 seconds. The aircraft did not touch the ground during either trial.

B. Transition to Free Flight

Once grasped, retrieving the object requires the helicopter to apply increased thrust to balance the weight of the payload

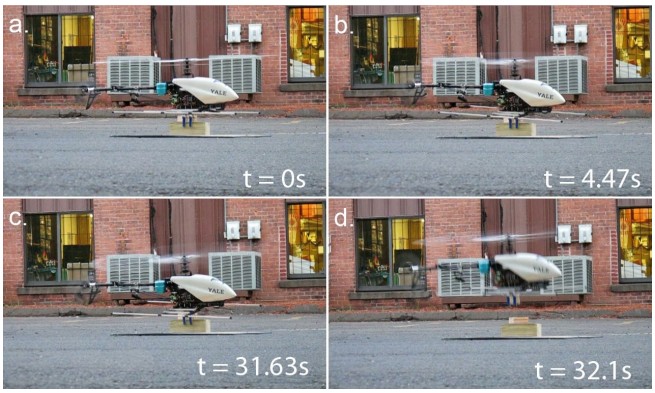

Fig. 14. Coupled hovering, grasping a block fixed to ground.

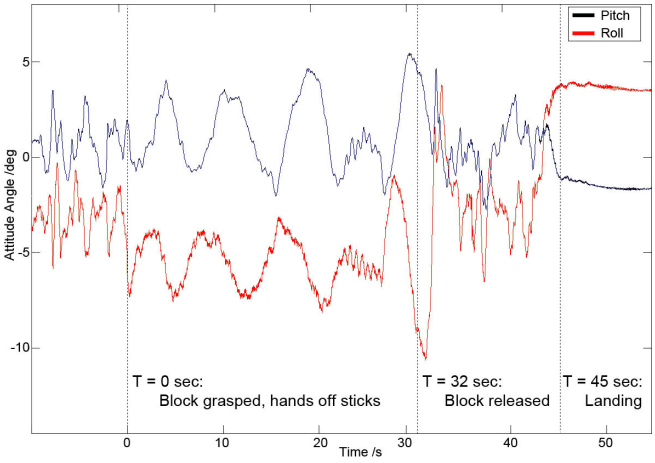

Fig. 15. Coupled hovering pitch and roll angles.

and transition to free flight. As the surface normal force reduces the lateral force produced by object contact friction will decrease — eventually the object slips, resulting in much reduced lateral stiffness. Similarly, the ground torque reaction decreases, devolving to single-point contact with only kinematic angular stiffness, until the payload begins to lift clear (Fig. 16).

Continued stability in partial contact depends on the object geometry and contact properties. A long flat object on ice will slide freely but hold the helicopter level, while a sticky rubber sphere on tarmac will act like a pin joint, potentially causing the helicopter to pivot into the ground.

In practice, transient contact conditions are difficult to maintain, due to the sensitivity of the helicopter to disturbances – as the applied thrust exceeds the net mass of the vehicle, the aircraft quickly loses contact with the ground. However, when grasping round objects, tractive objects with short base lengths, this transition should be made quickly so that instantaneous unstable conditions do not persist long enough to pose a danger to the aircraft.

C. Object Retrieval While Hovering

Complete operation of the Yale Aerial Manipulator was demonstrated by grasping and retrieving a variety of objects while hovering under PID control. Similar to the coupled grasping experiment, the helicopter was positioned over the

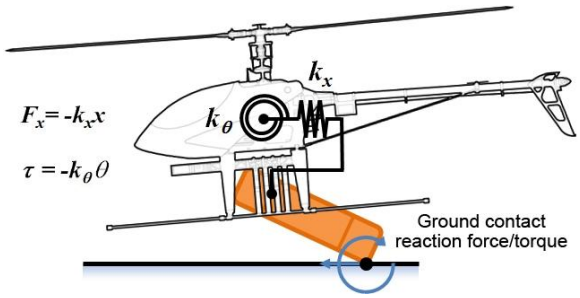

Fig. 16. Transitional contact force coupling model.

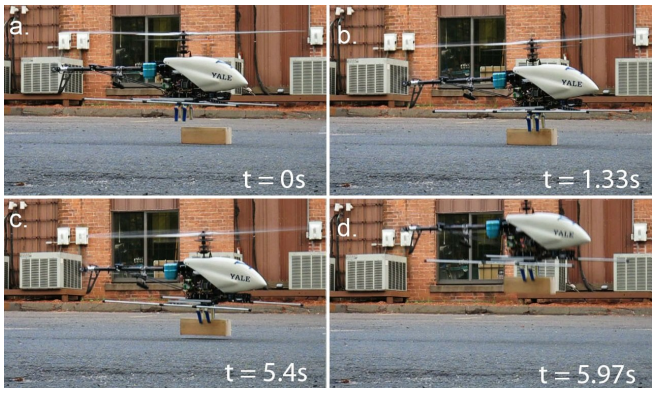

Fig. 17. Grasp and retrieval of a block while in hover.

target, switched to autonomous hover mode, and the gripper closed. Once the grasp was secure, rotor collective was increased until the object lifted clear of the ground (Fig. 17).

We have successfully demonstrated unstructured object retrieval 18 times; no trials exhibited instability, or caused the helicopter to touch the ground while grasping. Objects grasped include a wood block (700 g, 265 mm), PVC cylinder (900 g, 390 mm), softball (160 g, 89 mm), and a weighted tool case (1.45 kg, 335 mm, see Fig. 18). The block grasping and ground-coupled experiments described above are documented in the video attached to this paper.

VI. Conclusions

We have presented a planar helicopter model and analysis of attitude stability subject to bias and step disturbance encountered during the aerial grasping task. We have shown that under PID control, a helicopter will reject added load trim offsets, and that cyclic trim imitations dominate the range of allowable load positions; these load positions are within the range of expected grasp offsets. Experiments testing the response of a helicopter to trim imbalance demonstrated stability of the aircraft under these conditions.

Furthermore, we have examined the effect of transitional coupled hovering grasps as the aircraft picks up objects from the ground. We have verified the stability of a helicopter elastically coupled to a load for over 30 seconds. Finally, we have demonstrated successful object retrieval by a PID-stabilized teleoperated helicopter UAV 18 times, for a variety of object masses, sizes and shapes. To the authors' knowledge, this is the first instance of unstructured object retrieval with an aircraft-mounted gripper, while the aircraft is in flight.

Fig. 18. Yale aerial manipulator retrieving a 1.5 kg tool case.

VII. Acknowledgments

The authors would like to thank Joe Acosta of Build Right Fly Right Hobbies, Wallingford CT, USA, and Joseph Belter for their support of this work.

References

[1] D. Scott, M. Toal and J. Dale, "Vision Based Sensing for Autonomous In-flight Refueling," In Proc. of SPIE, Vol. 6561, 2007.

[2] M. Mammarella, G. Campa, M. Napolitano, M. Fravolini and R. Perhinschi, "Machine Vision/GPS Integration Using EKF for the UAV Aerial Refueling Problem," IEEE Transactions on Systems, Man and Cybernetics, Vol. 38, No. 6, 2008.

[3] M. Bisgaard, J. Bendtsen and A. la Cour-Harbo, "Modelling of Generic Slung Load System," Journal of Guidance, Control and Dynamics, Vol. 32, No. 2, 2009.

[4] R. Raz, A. Rosen and T. Ronen, "Active Aerodynamic Stabilization of a Helicopter/Sling-Load System," Journal of Aircraft, Vol. 26, No. 9, 1988.

[5] M. Bernard and K. Kondak, "Generic Slung Load Transportation System Using Small Size Helicopters," In Proc. IEEE International Conference on Robotics and Automation, 2009.

[6] N. Michael, J. Fink and V. Kumar, "Cooperative Manipulation and Transportation with Aerial Robots," In Proc. Robotic Science and Systems, 2009.

[7] O. Amidi, T. Kanade and J. Miller, "Vision-Based Autonomous Helicopter Research at Carnegie Mellon Robotics Institute 1991–1997," In Proc. American Helicopter Society International Conference, 1998.

[8] J. Borenstein, "The Hoverbot — An Electrically Powered Flying Robot," Unpublished paper, University of Michigan, 1992, http://www-personal.umich.edu/ johannb/hoverbot.htm (2009).

[9] N. Kuntz, and P. Oh, "Development of Autonomous Cargo Transport for an Unmanned Aerial Vehicle Using Visual Servoing," In Proc. Digital Systems and Control Conference, 2008.

[10] P.E.I. Pounds and A.M. Dollar, "Aerial Grasping from a Helicopter UAV Platform," In Proc. International Symposium on Experimental Robotics, 2010.

[11] P.E.I. Pounds and A.M. Dollar, "Hovering Stability of Helicopters With Elastic Tethers," In Proc. ASME Dynamic Systems and Control Conference, 2010.

[12] P.E.I. Pounds, P.I. Corke and R.E. Mahony, "Modelling and Control of a Large Quadrotor Robot," Control Engineering Practice, Vol. 18, No. 7, pp 691-699, 2010.

[13] Z. Yu, K. Nonami, J. Shin and D. Celestino, "3D Vision Based Landing Control of Small Scale Autonomous Helicopter," International Journal of Advanced Robotic Systems, Vol. 4, No. 1, 2007.

[14] A.M. Dollar and R.D. Howe, "The Highly Adaptive SDM Hand: Design and Performance Evaluation," Int. Journal of Robotics Research, Vol. 29, No. 5, pp 585-597, 2010.

[15] B. Mettler, Identification, Modeling and Characteristics of Miniature Rotorcraft, Kluwer Academics Publisher, Nowell, MA.

[16] R. Prouty, *Helicopter Performance, Stability, and Control*, Krieger Publishing Company, 2002.